Model Predictive Direct Power Control for a Grid-Connected Converter with an LCL-Filter

James Scoltock[1], Tobias Geyer[2], and Udaya Madawala[1]

[1]Department of Electrical and Computer Engineering, The University of Auckland, 1010 Auckland, New Zealand.
Email: jsco075@aucklanduni.ac.nz, u.madawala@auckland.ac.nz
[2]ABB Corporate Research, 5405 Baden-Dättwil, Switzerland. Email: t.geyer@ieee.org

***Abstract*—This paper presents a Model Predictive Direct Power Control (MPDPC) scheme for the control of a three-phase grid-connected Neutral Point Clamped (NPC) converter with an LCL-filter. MPDPC is a variant of Model Predictive Control (MPC) which regulates the output power of the converter within a set of hysteresis bounds, whilst minimising switching frequency and/or losses. By incorporating an Active Damping (AD) strategy which suppresses spectral content around the main resonant frequency of the LCL-filter, MPDPC achieves low levels of grid current distortion at low switching frequencies. Through simulation, it is shown that the proposed MPDPC strategy is capable of offering a significant improvement over the performance of Carrier-Based Pulse Width Modulation (CB-PWM) at the chosen steady-state operating points.**

***Index Terms*—Active damping, direct power control, grid connected converter, LCL-filter, model predictive control**

I. Introduction

In recent years, three-phase grid-connected Voltage-Source Converters (VSC) have been widely utilised, with important applications including the grid-integration of renewable energy systems and machine drive front ends. In Medium-Voltage (MV) applications, multi-level topologies such as the Neutral Point Clamped (NPC) converter are typically utilised, as they allow acceptable levels of output current distortion to be achieved with low switching frequencies.

Recently, Model Predictive Control (MPC) has gained popularity within the power electronics and drives community as a promising alternative to the established control paradigms, such as Field-Oriented Control (FOC) and Direct Torque Control (DTC). In MV applications, MPC is particularly attractive, as it has the potential to reduce the switching frequency and/or losses of the converter whilst maintaining acceptable levels of output distortion, or vice versa. Model Predictive Direct Torque Control (MPDTC) [1] - [3], and Model Predictive Direct Current Control (MPDCC) [4], are variants of MPC which have shown significant promise in MV machine drive applications. Model Predictive Direct Power Control (MPDPC) [5], which can be viewed as an extension of Direct Power Control (DPC), is a variant of MPC which directly controls the real and reactive power delivered and/or drawn by the converter. This makes MPDPC very well-suited to grid-connected applications, as the real and reactive power delivered to or drawn from the distribution system can be directly regulated.

In grid-connected applications, LC- and LCL-filters are widely utilised because of their ability to improve upon the harmonic attenuation offered by series inductors. The use of such filters, however, makes the control problem more challenging. Because the filter capacitance introduces a delay between the converter and the grid, it is difficult to directly control grid-side quantities, including real and reactive power. As such, multi-loop current control strategies used in conjunction with Pulse Width Modulation (PWM) are common [6], [7]. Moreover, when using strategies which present a spread output spectrum, such as DPC or MPDPC, the resonant frequency which is introduced by the filter needs to be adequately suppressed from the output of the converter [8], [9].

This paper outlines a modified MPDPC strategy for use with a three-phase grid-connected NPC converter with an LCL output filter. The proposed strategy is evaluated through MATLAB-based simulation. The performance is examined under steady-state conditions, and is compared against Carrier-Based PWM (CB-PWM) with multi-loop current control.

II. System Modelling

A representation of a three-phase NPC converter connected to the grid via an LCL-filter is shown in Fig. 1. It is assumed that the direction of current flow is from converter to grid and that the DC-link is fed from an ideal energy source, meaning that the DC-link voltage, V_{dc}, is constant.

A. $\alpha\beta$ Reference Frame

Variables $\xi_{abc} = [\xi_a \ \xi_b \ \xi_c]^T$ in the three-phase abc reference frame are transformed to $\xi_{\alpha\beta} = [\xi_\alpha \ \xi_\beta]^T$ in the orthogonal $\alpha\beta$ reference frame through

$$\xi_{\alpha\beta} = \frac{2}{3} P \xi_{abc} \tag{1}$$

where P is the transformation matrix

$$P = \begin{bmatrix} 1 & -\frac{1}{2} & -\frac{1}{2} \\ 0 & \frac{\sqrt{3}}{2} & -\frac{\sqrt{3}}{2} \end{bmatrix}. \tag{2}$$

It should be noted that (1) and (2) ignore the common-mode component of ξ_{abc}.

B. Converter Model

Each phase leg of the converter is able to assume one of three states, which can be represented by the integer variables $u_a, u_b, u_c \in \{-1, 0, 1\}$. Since there are three switching states per phase and three phases, there are $3^3 = 27$ possible switching states of the form $u_{abc} = [u_a \ u_b \ u_c]^T$. Within

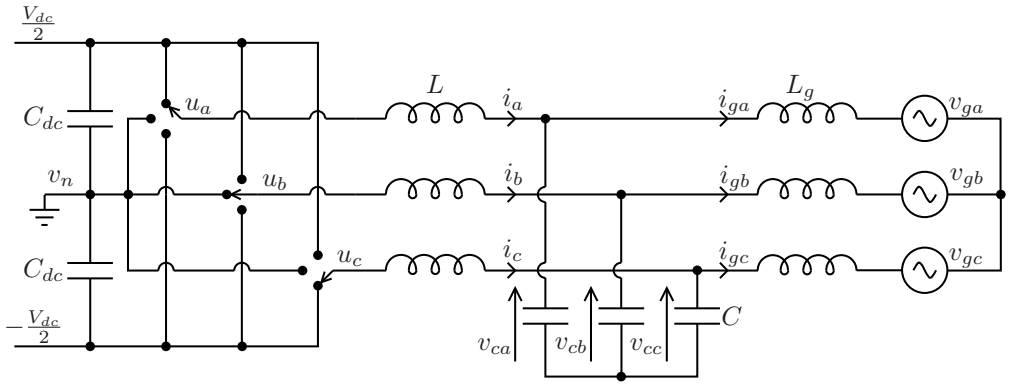

Fig. 1: Representation of a three-phase NPC converter connected to the grid via an LCL-filter.

those states there are 19 distinct voltage vectors, which can be represented by transforming the switching states from the three-phase abc-frame to the orthogonal $\alpha\beta$-frame, yielding vectors of the form $u_{\alpha\beta} = [u_\alpha \ u_\beta]^T$. The voltages as they appear across the output of the converter are given by

$$v_i = \frac{V_{dc}}{2} u_{\alpha\beta} \tag{3}$$

where $v_i = [v_{i\alpha} \ v_{i\beta}]^T$ and V_{dc} is the DC-link voltage. In the converter considered, all switching transitions are allowed except for those which involve switching between the upper and lower rails. For example, a transition from u_{abc} = [1 1 1]^T to [0 0 1]^T is allowed, whereas a transition to [-1 1 1]^T is not.

The neutral point potential, v_n, depends on the state of the converter. It is only affected when current is directly drawn from it when one or more of the switching states is zero. It follows that

$$\frac{dv_n}{dt} = -\frac{1}{2C_{dc}}((1-|u_a|)i_a + (1-|u_b|)i_b + (1-|u_c|)i_c) \tag{4}$$

where C_{dc} is the value of each of the two capacitors of the DC-link and i_a, i_b, i_c are the converter phase currents. Since it is assumed that $i_a + i_b + i_c = 0$, it follows that

$$\frac{dv_n}{dt} = \frac{1}{2C_{dc}} |u_{abc}|^T i_{abc} \tag{5}$$

where $|u_{abc}| = [|u_a| \ |u_b| \ |u_c|]^T$ and $i_{abc} = [i_a \ i_b \ i_c]^T$.

C. LCL-Filter Model

A model which expresses the dynamics of the LCL-filter on a per-phase basis is required. As such, suitable inputs and states need to be defined. With the filter modelled in the $\alpha\beta$ reference frame, the state vector can be expressed in terms of the converter current, grid current, capacitor voltage and grid voltage as

$$x = [i^T \ i_g^T \ v_c^T \ v_g^T]^T \tag{6}$$

with the converter current i = $[i_\alpha \ i_\beta]^T$, the grid current i_g = $[i_{g\alpha} \ i_{g\beta}]^T$, the capacitor voltage v_c = $[v_{c\alpha} \ v_{c\beta}]^T$, and the grid voltage v_g = $[v_{g\alpha} \ v_{g\beta}]^T$. With the input vector defined as the converter voltage v_i and the output vector defined as the instantaneous real and reactive power, y = $[p \ q]^T$, the continuous-time state and output equations of the system are given by

$$\frac{dx}{dt} = Ax + Bv_i \tag{7}$$

$$y = g(x) \tag{8}$$

where A is the state matrix, B is the input matrix, and $g(x)$ is the output function, all of which are defined in the appendix.

III. Model Predictive Direct Power Control

A. Control Problem

The aim of DPC, and by extension MPDPC, is to keep the real and reactive power delivered to the grid within hysteresis bounds of width $\pm\delta_p$ and $\pm\delta_q$, respectively. Moreover, when an NPC converter is used, the controller must keep the neutral point potential within a set of hysteresis bounds of width $\pm\delta_{NP}$. Total Demand Distortion (TDD), which expresses the sum of the harmonic components of a particular quantity as a percentage of the nominal fundamental component [4], is used to measure output distortion.

Because the filter capacitance makes the direct control of grid-side quantities difficult, the instantaneous real and reactive grid power cannot be directly controlled in a straightforward manner. As such, the real and reactive power are defined in terms of deterministic and/or easily controllable variables. Based on the conventional definitions of real and reactive power and using the grid voltage $v_{g\alpha\beta}$ and the converter current $i_{\alpha\beta}$, the real and reactive power to be controlled can be defined as

$$p = \frac{3}{2}(v_{g\alpha} i_\alpha + v_{g\beta} i_\beta) \tag{9}$$

$$q = \frac{3}{2}(v_{g\beta} i_\alpha - v_{g\alpha} i_\beta) \tag{10}$$

where p and q are the instantaneous real and reactive power, respectively.

In addition to regulating the output variables within their respective hysteresis bounds, MPDPC aims to minimise the switching losses of the converter. This can be achieved indirectly, by minimising the converter switching frequency, or directly, by estimating and minimising the switching losses of the converter.

B. Internal Model of the Controller

In order for the controller to make predictions of future states and outputs, a discrete-time model which unifies the

converter and LCL-filter models is required. By re-defining the input and state vectors in discrete-time as

$$u(k) = [u_a(k)\ u_b(k)\ u_c(k)]^T \tag{11}$$

and

$$x(k) = [i(k)^T\ i_g(k)^T\ v_c(k)^T\ v_g(k)^T\ v_n(k)]^T \tag{12}$$

and defining the discrete-time output vector as

$$y(k) = [p(k)\ q(k)\ v_n(k)]^T \tag{13}$$

a complete model of the system can be derived by applying either exact or forward-Euler discretization to (5), (7) and (8). Due to space constraints the full internal control model cannot be included. Further details regarding the formulation of the internal control model for MPDPC are included in [5].

C. MPDPC Control Procedure

The MPDPC control procedure is the same as the generalised MPDTC algorithm discussed in [3], with the only difference between the two being the formulation of the internal control model.

Beginning at the current time-step k, the algorithm predicts the state and output trajectories forward in time for each allowable switching sequence. Each sequence must remain a *candidate* at each step of the prediction in order to be considered during the subsequent optimisation process. A candidate sequence is one for which each output is either *feasible* (within its respective bounds) or *pointing in the proper direction* (outside its bounds, but moving closer to them).

Predictions are controlled by the *switching horizon*, N_s, which is made up of a fixed number of 'S' (switch) and 'E' (extend) events. The fixed switching horizon gives rise to a *prediction horizon*, N_p, of variable length. Consider the switching horizon 'SSE', which involves switching at time-steps k and $k+1$, and subsequent extension of the output trajectories until time-step $k+N_p$, at which point the trajectories cannot be extended any further without violating candidacy constraints. Depending on the exact sequence of switching states and the width of the hysteresis bounds, the prediction horizon N_p may range from a few time-steps to several dozen time-steps. An additional 'e' event can also be added to the beginning of the switching horizon, denoting an optional extension event.

The MPDPC control procedure can be summarised as follows, using the switching horizon 'SESE' as an example:

1) Carry out the first 'S' event by predicting the states and outputs at $k+1$ for each switching state which can be applied at k. The allowable switching states at k are determined by the switching constraints of the converter and the previous input $u(k-1)$.
2) Carry out the first 'E' event by extending each trajectory forward in time until one or more of the outputs cannot be extended any further without violating candidacy constraints. Trajectory extension can be performed using the internal control model, or with an extrapolation or interpolation technique [10].
3) Carry out the second 'S' event in the same manner as the first.
4) Carry out the second 'E' event in the same manner as the first.
5) For each candidate sequence $U^i(k) = [u^i(k), u^i(k+1), ..., u^i(k+N_p^i-1)]$, where $i \in \mathcal{I}$ and $\mathcal{I}$ is an index set, calculate the associated cost. This is given by

$$c^i = \frac{1}{N_p^i} \sum_{\ell=k}^{k+N_p^i-1} \|u^i(\ell) - u^i(\ell-1)\|_1 \tag{14}$$

for minimisation of switching frequency, or

$$c^i = \frac{E^i}{N_p^i} \tag{15}$$

for minimisation of switching losses. Here E is the total switching energy loss over the prediction horizon. A detailed description of the calculation of switching losses is given in [3].
6) Determine the switching sequence with the minimal cost

$$i = \arg\min_{i \in \mathcal{I}} c^i. \tag{16}$$

7) Apply the switch position $u(k) = u^i(k)$ and shift the horizon one step forward.

The MPDPC algorithm is repeated at the next time-step, with a new optimal switching state $u(k+1)$ determined. For further details regarding the control procedure, the reader is referred to [1], [3].

Because of the computational burden associated with the MPDPC algorithm, the use of advanced mathematical techniques may be necessary in a practical setting. In particular, the use of branch and bound optimisation, as discussed in [11], has been shown to reduce the computational effort of MPDTC by an order of magnitude, and could similarly be applied to MPDPC.

IV. Active Damping

Although the LCL-filter offers a higher level of harmonic attenuation than series inductance, it presents additional challenges in the regulation of output power. In addition to the delay between the converter and grid, the LCL-filter possesses resonant frequencies at

$$\omega_1 = \frac{1}{\sqrt{CL_g}} \tag{17}$$

$$\omega_2 = \frac{1}{\sqrt{C\frac{LL_g}{L+L_g}}}. \tag{18}$$

In particular, the resonant frequency ω_1 requires damping, as it is the frequency at which resonance between the converter- and grid-side currents occurs.

Passive damping with series- or parallel-connected resistors, as shown in Fig. 2, is a straightforward but inefficient damping strategy. As such, numerous Active Damping (AD) strategies have been proposed. The *Virtual Resistor* (VR) strategy, as outlined in [12], [13], emulates the effect of adding a physical damping resistor(s) to the filter, without the associated power loss. Unlike the series resistors R_1, R_3 and R_5, the VR strategy is able to emulate the effects of the parallel resistors R_2, R_4 and R_6 without the use of a differentiator. This means that their implementation is straightforward, as knowledge of the system is required at the current time-step only, eliminating the

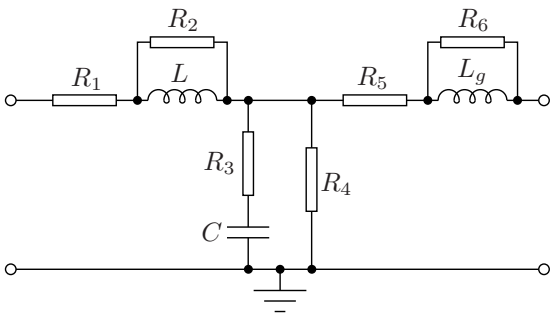

Fig. 2: Possible locations for passive damping resistors in an LCL-filter.

need for the storage of previous states. The chosen damping strategy incorporates the effects of R_2 and R_4, both of which assist in damping the resonant frequency ω_1. The additive converter current damping component, i^*_{vr}, is subsequently given by

$$i^*_{vr} = \frac{i}{R_{v2}} - \frac{v_c}{R_{v4}} \tag{19}$$

where $i^*_{vr} = [i^*_{vr\alpha}\ i^*_{vr\beta}]^T$, R_{v2} is the value of the VR emulating R_2, and R_{v4} is the value of the VR emulating R_4. Because MPDPC requires power references, i^*_{vr} is multiplied by the grid voltage v_g to give the real and reactive power damping components

$$p^*_{vr} = \frac{3}{2}(v_{g\alpha} i^*_{vr\alpha} + v_{g\beta} i^*_{vr\beta}) \tag{20}$$

and

$$q^*_{vr} = \frac{3}{2}(v_{g\beta} i^*_{vr\alpha} - v_{g\alpha} i^*_{vr\beta}). \tag{21}$$

An outer AD block calculates the damping components at each time-step k based on measured state variables. After the DC-quantities $p^*_{vr,dc}(k)$ and $q^*_{vr,dc}(k)$ of $p^*_{vr}(k)$ and $q^*_{vr}(k)$ are removed, the damping components are added to the fundamental references $p^*_f(k)$ and $q^*_f(k)$, to give the overall references $p^*(k)$ and $q^*(k)$.

Although it is not unreasonable to assume fixed references over the course of a prediction in the case of short horizons such as 'eSE', it can degrade the performance of the controller when longer horizons are used. As such, the references $p^*(k)$ and $q^*(k)$ need to be predicted along with the states and outputs as part of the MPDPC algorithm. The most obvious way this could be done is by updating the references at every time-step ℓ of the prediction, based on the predicted state $x(\ell)$, with $\ell = k, ..., k + N_p$. However, this strategy presents several drawbacks; in addition to increasing the computational burden of the control procedure, it is only feasible when exact extension is used.

To overcome this, the references are updated only at each 'S' event within each prediction. This approach does not add significantly to the complexity of the algorithm. Moreover, it means that when the bounds require updating the predicted states are always known, whether using exact extension or extrapolation. If switching occurs at time-step ℓ, then the damping components $p^*_{vr}(\ell)$ and $q^*_{vr}(\ell)$ are given by

$$p^*_{vr}(\ell) = \frac{3}{2}(v_{g\alpha}(\ell) i_{vr\alpha}(\ell)^* + v_{g\beta}(\ell) i_{vr\beta}(\ell)^*) \tag{22}$$

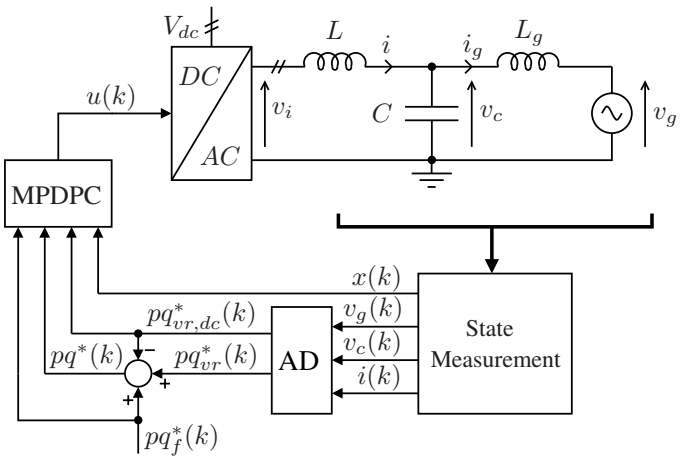

Fig. 3: Control structure for MPDPC with Active Damping (AD).

and

$$q^*_{vr}(\ell) = \frac{3}{2}(v_{g\beta}(\ell) i_{vr\alpha}(\ell)^* - v_{g\alpha}(\ell) i_{vr\beta}(\ell)^*). \tag{23}$$

After $p^*_{vr}(\ell)$ and $q^*_{vr}(\ell)$ are added to $p^*_f(k)$ and $q^*_f(k)$, the DC-components calculated by the outer AD block are removed, giving $p^*(\ell)$ and $q^*(\ell)$. Fig. 3 shows the overall control structure for MPDPC with active damping.

V. Performance Evaluation

A. Case Study

The performance of the proposed control strategy has been evaluated through a MATLAB-based simulation of the system described in Sect. II. The semiconductor models which have been used for the NPC converter are based on the ABB 35L4510 4.5 kV 4 kA Integrated Gate Commutated Thyristor (IGCT) and the ABB 10H4520 fast recovery diode. The LCL-filter has a resonant frequency ω_1 of about 1290 rads^{-1} (205 Hz). The value of the filter capacitor C is 1 mF, whilst the inductors are $L = L_g = 600\ \mu$H, both with a series resistance of 5 mΩ. The per-unit system, which is used in all simulations, is established from foundation values of $V_{base} = \sqrt{2/3} V_g = 2449$ V, $P_{base} = 8$ MVA and $f_{base} = 50$ Hz. A summary of nominal ratings and per-unit (p.u.) parameters is shown in Table I.

All MPDPC simulations have been run with a sampling time of 25 μs, with a neutral point bound width $\delta_{NP} = 0.03$ p.u. The cost function has been formulated to penalise converter switching losses. The value of the VRs R_{v2} and R_{v4} are set to 1.2 p.u. and 4.5 p.u, respectively. The fundamental real and reactive power references are set to $p^*_f = 0.933$ p.u. and $q^*_f = -0.356$ p.u, in order to deliver 1 p.u. real power and 0 p.u. reactive power to the grid.

TABLE I: Nominal ratings (left) and p.u. parameters (right) of the system.

Grid & LCL-Filter			
Grid voltage, V_g	3000 V	L, L_g	0.168 p.u.
Grid current, I_g	1540 A	R, R_g	0.004 p.u.
Grid frequency, f	50 Hz	C	0.353 p.u.
Converter			
DC-link voltage	5200 V	C_{dc}	3.534 p.u.
Apparent power	8 MVA		

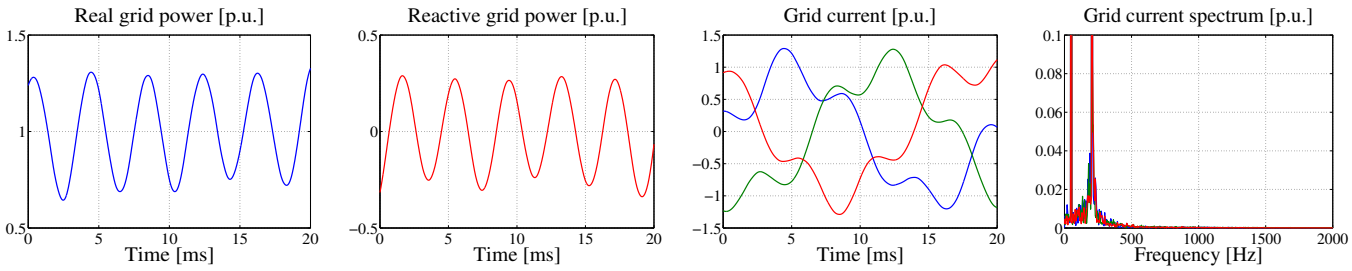

Fig. 4: Steady-state real and reactive grid power, grid current, and grid current spectrum for MPDPC with no active damping over one fundamental.

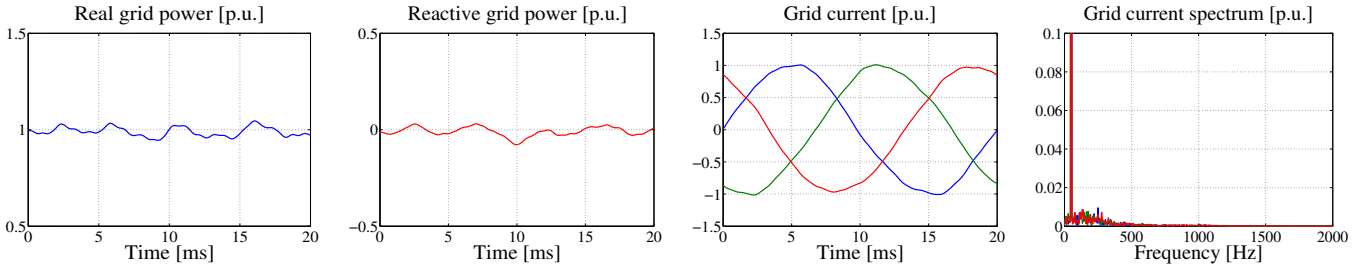

Fig. 5: Steady-state real and reactive grid power, grid current, and grid current spectrum for MPDPC with active damping included over one fundamental.

B. Active Damping Performance

Fig. 4 shows the real and reactive power delivered to the grid, along with the grid current and spectrum, for MPDPC with no AD strategy in place. As can be seen, significant harmonic content is present in the output, centred around the main LCL-filter resonant frequency of 205 Hz. With bound widths of δ_p = 0.12 p.u. and δ_q = 0.08 p.u. and N_s = 'eSE', the TDD of the grid current is 38%. Fig. 5 shows the same quantities after the AD strategy described in Sect. IV is introduced. As can be seen, the AD strategy is very effective in suppressing the spectral content around the resonant frequency, resulting in smoother power delivery and much lower current TDD. With the same bound widths and switching horizon, the AD strategy reduces the TDD of the grid current to 3.1%. The evolution of the real and reactive power with the AD strategy included is shown over one fundamental in Fig. 6.

C. Steady-State Performance Comparison

The steady state performance of MPDPC is benchmarked against Carrier-Based Pulse Width Modulation (CB-PWM) with multi-loop current control in Table II. The chosen CB-PWM strategy is regular sampled with Phase-Disposition (PD) of the triangular carriers. Moreover, a min/max common mode component is added to the reference to increase the output range. The CB-PWM scheme includes the same outer-loop active damping strategy as MPDPC. The comparison is made with fixed device switching losses of around 20 kW, and with a fixed grid current TDD of around 3%. At both operating points the device switching frequencies are in the range of 300 - 450 Hz, which is in the typical range for a MV NPC converter.

With the switching losses fixed at about 20 kW, MPDPC with N_s = 'eSE' presents a grid current TDD which is around 11% higher than CB-PWM. By extending the horizon to 'eSESE', however, the TDD is reduced by 7.4% relative to CB-PWM. By further lengthening the horizon to 'eSSESE', the TDD is reduced by around 13.9% relative to CB-PWM. This is a significant improvement, and highlights the advantage of lengthening the switching horizon, and therefore prediction horizon, of MPDPC.

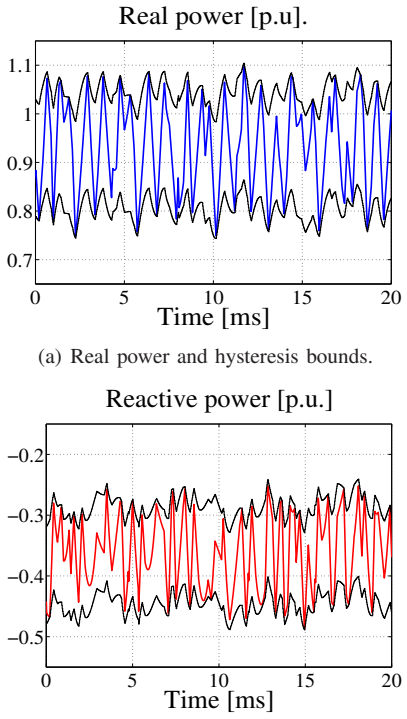

(a) Real power and hysteresis bounds.

(b) Reactive power and hysteresis bounds.

Fig. 6: Evolution of the real and reactive power, and the respective hysteresis bounds, over one fundamental.

TABLE II: Comparison of MPDPC with CB-PWM. The first comparison is made with fixed switching losses of about 20 kW, whilst the second is made with a fixed grid current TDD of around 3%. The second column shows absolute values whilst the third shows values relative to CB-PWM. f_c denotes the carrier frequency for CB-PWM, P_{sw} the average device switching losses, and f_{sw} the average device switching frequency. The bounds δ_p and δ_q are expressed as per-unit (p.u.) quantities.

Control scheme	Control setting	Switching horizon	Average prediction horizon (time-steps)	$i_{g,TDD}$ [%]	P_{sw} [kW]	f_{sw} [Hz]	$i_{g,TDD}$ [%]	P_{sw} [%]	f_{sw} [%]
CB-PWM	f_c = 550 Hz	-	-	3.80	20.0	300	100	100	100
MPDPC	δ_p = 0.160, δ_q = 0.090	eSE	12.2	4.23	20.5	348	111	103	116
MPDPC	δ_p = 0.160, δ_q = 0.080	eSESE	25.7	3.52	20.1	339	92.6	101	113
MPDPC	δ_p = 0.144, δ_q = 0.082	eSSESE	28.3	3.27	19.1	321	86.1	95.5	107
CB-PWM	f_c = 700 Hz	-	-	2.98	25.5	375	100	100	100
MPDPC	δ_p = 0.100, δ_q = 0.086	eSE	9.8	3.01	26.3	450	101	103	120
MPDPC	δ_p = 0.120, δ_q = 0.080	eSESE	22.5	3.06	22.7	364	103	89.0	97.1
MPDPC	δ_p = 0.120, δ_q = 0.080	eSSESE	25.9	3.07	21.1	352	103	82.7	93.9

With the grid current TDD fixed at around 3%, the losses of MPDPC with N_s = 'eSE' are around 3% higher than CB-PWM. By increasing the horizon to 'eSESE', MPDPC improves on the losses of CB-PWM by around 11%. With the horizon extended to 'eSSESE', MPDPC is able to reduce the losses by around 17.3%, which equates to around 4.4 kW per switch.

VI. Conclusion

This paper has presented a modified MPDPC strategy for the control of a three-phase grid-connected NPC converter with an LCL output filter. The converter and LCL-filter have been modelled, and the proposed active damping strategy, which is based on the virtual resistor concept, has been outlined. The performance of the proposed strategy has been evaluated through simulation and benchmarked against CB-PWM with multi-loop current control. With the device switching losses fixed to around 20 kW, MPDPC with a switching horizon of 'eSSESE' reduces the grid current TDD by around 13.9% relative to CB-PWM. Furthermore, with the grid current TDD held constant to around 3%, MPDPC with the same switching horizon is able to reduce the average device switching losses by about 17.3% relative to CB-PWM.

Acknowledgment

This work was supported by The University of Auckland Doctoral Scholarship.

Appendix

The matrices for the state and output equations (7), (8) are as follows

$$A = \begin{bmatrix} \frac{-R}{L} & 0 & 0 & 0 & \frac{-1}{L} & 0 & 0 & 0 \\ 0 & \frac{-R}{L} & 0 & 0 & 0 & \frac{-1}{L} & 0 & 0 \\ 0 & 0 & \frac{-R_g}{L_g} & 0 & \frac{1}{L_g} & 0 & \frac{-1}{L_g} & 0 \\ 0 & 0 & 0 & \frac{-R_g}{L_g} & 0 & \frac{1}{L_g} & 0 & \frac{-1}{L_g} \\ \frac{1}{C} & 0 & \frac{-1}{C} & 0 & 0 & 0 & 0 & 0 \\ 0 & \frac{1}{C} & 0 & \frac{-1}{C} & 0 & 0 & 0 & 0 \\ 0 & 0 & 0 & 0 & 0 & 0 & 0 & -\omega \\ 0 & 0 & 0 & 0 & 0 & 0 & \omega & 0 \end{bmatrix} \quad (24)$$

$$B = \begin{bmatrix} \frac{1}{L} & 0 & 0 & 0 & 0 & 0 & 0 & 0 \\ 0 & \frac{1}{L} & 0 & 0 & 0 & 0 & 0 & 0 \end{bmatrix}^T \quad (25)$$

$$g(x) = \begin{bmatrix} \frac{3}{2}(x_7 x_1 + x_8 x_2) \\ \frac{3}{2}(x_8 x_1 - x_7 x_2) \end{bmatrix} \quad (26)$$

where L and R are the converter-side inductance and series resistance, L_g and R_g are the grid-side inductance and series resistance, C is the filter capacitance, and ω is the angular frequency of the grid voltage.

References

[1] T. Geyer, G. Papafotiou, and M. Morari. Model predictive direct torque control - part I: Concept, algorithm and analysis. *IEEE Trans. Ind. Electron.*, 56(6):1894–1905, Jun. 2009.

[2] G. Papafotiou, J. Kley, K.G. Papadopoulos, P. Bohren, and M. Morari. Model predictive direct torque control - part II: Implementation and experimental evaluation. *IEEE Trans. Ind. Electron.*, 56(6):1906–1915, Jun. 2009.

[3] T. Geyer. Generalized model predictive direct torque control: Long prediction horizons and minimization of switching losses. In *Proc. IEEE Conf. Decis. Control*, pages 6799 – 6804, Shanghai, China, Dec. 2009.

[4] T. Geyer. Model predictive direct current control: Formulation of the stator current bounds and the concept of the switching horizon. *IEEE Ind. Appl. Mag.*, 18(2):47–59, Mar. 2012.

[5] T. Geyer, J. Scoltock, and U. Madawala. Model predictive direct power control for grid-connected converters. In *Proc. IEEE Ind. Electron. Soc. Conf.*, pages 1438 – 1443, Melbourne, Australia, Nov. 2011.

[6] E. Twining and D.G. Holmes. Grid current regulation of a three-phase voltage source inverter with an LCL input filter. *IEEE Trans. Power Electron.*, 18(3):888 – 895, May 2003.

[7] P.C. Loh and D.G. Holmes. Analysis of multiloop control strategies for LC/CL/LCL-filtered voltage-source and current-source inverters. *IEEE. Trans. Ind. Appl.*, 41(2):644 – 654, Mar./Apr. 2005.

[8] L.A. Serpa, S.D. Round, and J.W. Kolar. A virtual-flux decoupling hysteresis current controller for mains inverter systems. *IEEE Trans. Power Electron.*, 22(5):1766 – 1777, Sep. 2007.

[9] L.A. Serpa, S. Ponnaluri, P.M. Barbosa, and J.W. Kolar. A modified direct power control strategy allowing the connection of three-phase inverters to the grid through LCL filters. *IEEE. Trans. Ind. Appl.*, 43(5):1388 – 1400, Sep./Oct. 2007.

[10] Y. Zeinaly, T. Geyer, and B. Egardt. Trajectory extension methods for model predictive direct torque control. In *Proc. IEEE Appl. Power Electron. Conf. Expo.*, pages 1667 – 1674, Fort Worth, USA, Mar. 2011.

[11] T. Geyer. Computationally efficient model predictive direct torque control. *IEEE Trans. Power Electron.*, 26(10):2804–2816, Oct. 2011.

[12] P.A. Dahono, Y.R. Bahar, Y. Sato, and T. Kataoka. Damping of transient oscillations on the output LC filter of PWM inverters by using a virtual resistor. In *Proc. IEEE Power Electron. Drive Syst. Conf.*, pages 403 – 407, Bali, Indonesia, Oct. 2001.

[13] P.A. Dahono. A control method to damp oscillation in the input LC filter of AC-DC PWM converters. In *Proc. IEEE Power. Electron. Spec. Conf.*, pages 1630 – 1635, Cairns, Australia, Jun. 2002.